Biophysical Journal Volume 94 March 2008 2115–2127

Oligomerization of Membrane-Bound Diphtheria Toxin (CRM197) Facilitates a Transition to the Open Form and Deep Insertion

M. S. Kent,* H. Yim,* J. K. Murton,* S. Satija,† J. Majewski,‡ and I. Kuzmenko§
*Sandia National Laboratories, Albuquerque, New Mexico; †National Institute of Standards and Technology, Gaithersburg, Maryland; ‡Los Alamos Neutron Science Center, Los Alamos, New Mexico; and §Advanced Photon Source, Argonne National Labs, Argonne, Illinois

ABSTRACT Diphtheria toxin (DT) contains separate domains for receptor-specific binding, translocation, and enzymatic activity. After binding to cells, DT is taken up into endosome-like acidic compartments where the translocation domain inserts into the endosomal membrane and releases the catalytic domain into the cytosol. The process by which the catalytic domain is translocated across the endosomal membrane is known to involve pH-induced conformational changes; however, the molecular mechanisms are not yet understood, in large part due to the challenge of probing the conformation of the membrane-bound protein. In this work neutron reflection provided detailed conformational information for membrane-bound DT (CRM197) in situ. The data revealed that the bound toxin oligomerizes with increasing DT concentration and that the oligomeric form (and only the oligomeric form) undergoes a large extension into solution with decreasing pH that coincides with deep insertion of residues into the membrane. We interpret the large extension as a transition to the open form. These results thus indicate that as a function of bulk DT concentration, adsorbed DT passes from an inactive state with a monomeric dimension normal to the plane of the membrane to an active state with a dimeric dimension normal to the plane of the membrane.

INTRODUCTION

Many bacterial toxins act by enzymatically modifying substrates in the cytosol of mammalian cells. The mechanisms by which the enzymes reach the cytosol are generally poorly understood. Diphtheria toxin (DT) is produced by strains of *Corynebacterium diphtheriae* infected by the lysogenic bacteriophage corynephage β and is perhaps the most well studied of the bacterial toxins (1–5). It is composed of three folded domains: a catalyst (C) domain composed of residues 1–186 on the N-terminus, a translocation (T) domain composed of residues 202–378, and a receptor domain (R) on the C-terminal end composed of residues 386–535. DT binds to a wide range of mammalian cell types displaying the heparin-binding EGF-like growth factor (HB-EGF) receptor. After binding it is taken up into endosome-like acidic compartments by the clatherin-coated pathway, where upon acidification (pH 5.0–5.3) the T domain inserts into the endosomal membrane and releases the C domain into the cytosol of the infected cell. The detailed molecular mechanism by which the C domain is translocated across the membrane is not understood. Understanding the translocation mechanism will greatly facilitate ongoing efforts to redesign this toxin for therapeutic purposes (1,6–10).

Much has been learned about DT and its interaction with lipid membranes through the careful studies of many groups (1,2,11). Crystal structures have been reported for the full wild-type toxin in monomeric form (at 2.3 Å 1MDT (12); at 1.55 Å 1FOL (13)) and in R domain-swapped dimeric form (1DDT (14)) for the full toxin in dimeric form bound to an extracellular fragment of its receptor HB-EGF (1XDT (15)) and for the C domain (1DTP (16)). The approximate dimensions of the monomer in the closed form are (78 Å × 35 Å × 53 Å), and those of the R domain-swapped dimer in the closed form are (110 Å × 35 Å × 53 Å). Under some conditions DT adopts an open form in which the R domain is separated from the C- and T domains (15). The role of this conformation in facilitating interaction of the T domain with the membrane has been unclear.

The T domain alone has been shown to be sufficient to translocate the C domain (17). The T domain consists of 10 helices in 3 rows. The innermost layer is a hairpin of helices 8 and 9 (TH8, TH9) bridged by an acidic loop. TH8 and TH9 are the most hydrophobic of the helices, and play a major role in the insertion process (18,19). Much work has been devoted to determining the conformation of the T domain imbedded in the membrane. In membranes at low pH, the T domain can exist in either a shallow or deeply penetrating conformation depending upon T domain concentration in the membrane and the length of the lipid tails (20,21). In the deeply inserted transmembrane state, evidence indicates that the C domain and the amino terminal third of the T domain, the first 270 residues, are translocated. TH5, TH8, TH9 are transmembrane whereas TH6-TH7 lie parallel within the headgroups on the *cis* side (22).

Despite this progress and other work reviewed elsewhere (1,2,11), many important questions remain regarding the translocation process. Conflicting conclusions have been reported for many important aspects, such as whether oligomerization of DT is critical for translocation (18,20,23–26) or not (27), whether the C domain must unfold to be translocated (28,29) or not (30), whether interaction of C with inserted T is critical to translocation (31) or not (30), and whether voltage-driven channel formation in planar bilayers is directly related to

Submitted May 24, 2007, and accepted for publication October 16, 2007.
Address reprint requests to M. S. Kent, E-mail: mskent@sandia.gov.
Editor: Klaus Schulten.

0006-3495/08/03/2115/13 $2.00
doi: 10.1529/biophysj.107.113498

translocation (17–19,22,26,27,30,32) or not (33). Much of this confusion is likely due to differences in the systems studied, such as differences in toxin concentration, whether the full toxin or only portions were used, whether the systems were driven primarily by pH or also included an electrostatic potential, and whether or not the HB-EGF receptor was present. However, resolving these questions is especially challenging because of the difficulty of obtaining direct structural data on the conformational states of the full toxin as it interacts with lipid membranes. To date, structural information has been obtained from fluorescence methods (20,31,34–37), from locating particular residues on either side of the bilayer membrane (17,22), from detecting changes in secondary and tertiary structure using circular dichroism (17,35) or infrared spectroscopy (38), and from the effects of mutations of specific residues on channel formation as detected by electrical current or the passage of reporter molecules (36). These methods have contributed many important insights, but the picture is still far from complete.

In this work, we used neutron reflection (NR) to supply direct structural information for the entire toxin (in contrast to methods that provide information only for labeled residues or secondary structural elements) as it adsorbs to planar lipid membranes and subsequently undergoes pH-dependent conformational changes to insert and translocate the enzyme. NR probes the in-plane averaged scattering length density (SLD) profile normal to the membrane, which is a function of the density and atomic composition (39,40) and therefore provides the one-dimensional envelope of the entire protein. The resolution (~7–10 Å in the best cases) is not at the atomic level as in x-ray crystallography; yet it is still sufficient to resolve different domains of a protein and to provide structural detail within each domain, particularly when selective deuteration is employed. Although specular reflectivity does not probe in-plane structure, it is sensitive to any structural changes that alter the profile normal to the membrane. The NR studies were complemented by x-ray reflectivity (XR) and grazing incidence x-ray diffraction (GIXD) measurements, which are very sensitive to membrane insertion processes. As discussed below, the NR studies indicate that membrane-bound DT oligomerizes as a function of DT concentration and has a dimension normal to the plane of the membrane consistent with a dimer. This is an important new insight, as previous discussions have considered only lateral assembly of DT in the plane of the membrane. Finally, the data strongly suggest that oligomerization facilitates a transition from the closed to the open form upon decrease in pH that coincides with insertion of residues into the lipid tails.

MATERIALS AND METHODS

Materials

These studies involved CRM197, which is a mutant form of DT that results from the substitution of glutamic acid for glycine at amino acid 52 in the C domain, rendering the protein nontoxic. CRM197 was purchased from EMD Biosciences (San Diego, CA). 1,2-Dipalmitoyl-*sn*-glycero-3-[phospho-rac-(1-glycerol)] (DPPG) and a deuterated form of DPPG in which the 62 protons in the aliphatic tails were replaced with deuterons (d-DPPG) were purchased from Avanti (Alabaster, AL). The phosphoric acid buffer (pH 7.3) was prepared by dissolving 8.16 g sodium hydrogen phosphate heptahydrate (Aldrich, Milwaukee, WI), 1.20 g sodium dihydrogen phosphate monohydrate (Aldrich), and 5.86 g sodium chloride (Aldrich) in 1 L of Millipore water (18 MΩ resistivity; Millipore, Bedford, MA). Chloroform and citric acid were purchased from Aldrich. All materials were used as received.

Adsorption studies

In a typical adsorption run, DPPG was spread in the form of a monolayer to a surface pressure of 1–3 mN/m on the surface of phosphate-buffered subphase (pH 7.3) held within a Teflon trough. DPPG was used because the T domain is known to bind to and insert into negatively charged membranes (20,22). After allowing the chloroform to evaporate, the surface layer was compressed to 30 mN/m and maintained at that value for the remainder of the run by a feedback system that adjusted the surface area through a sliding barrier. After collecting NR, XR, or GIXD data for the lipid monolayer alone, CRM197 was introduced into the subphase using a peristaltic pump and Teflon tubing with an inlet and outlet submerged at opposite ends of the trough. The desired amount of protein solution was first injected into a small vial using a 1 ml syringe, and then the solution was pumped from the vial into the trough using the peristaltic pump and a three-way Teflon valve. The subphase was then circulated at least twice to achieve complete mixing. NR showed little or no adsorption of DT at neutral pH over the concentration range studied. The pH of the subphase was then incrementally decreased by adding aliquots of citric acid. After addition of citric acid, the subphase was circulated to ensure thorough mixing. The circulation was then halted and NR, XR, or GIXD data were collected in successive scans until no further change was detected on a timescale of several hours. The pH of the subphase was measured before and after the reflectivity scans on a small volume (several ml) removed from the subphase using the three-way valve. The reported values are the averages of the two measurements, which typically deviated by <0.1 pH unit. For all measurements the trough was contained inside a closed canister to minimize evaporation. To reduce the amount of protein needed, a small Teflon trough (~40 mls) was used, which was placed inside the standard troughs available at the beamlines. The measurements were made at 23°C ± 3°C.

Neutron reflection

Reflectometry involves measuring the ratio of reflected to incident intensity as a function of momentum transfer $q_z = 4\pi\sin\theta/\lambda$, where θ is the angle of incidence relative to the plane of the membrane and λ is the wavelength. Manipulating the contrast between various components is integral to neutron scattering approaches. For organic materials this is readily accomplished using the very different neutron scattering properties of hydrogen and deuterium. In particular, this work involved the use of h-DPPG and d-DPPG. Neutron reflectometry was performed on the NG7 (NCNR/NIST) and SPEAR (LANSCE/LANL) reflectometers. The reflectivity data were analyzed using the GAFIT program based on the optical matrix method (39). GAFIT is available at www.ncnr.nist.gov. Simultaneous fits were performed for several sets of data at the two contrast conditions (h-DPPG and d-DPPG). In the simultaneous fits, the lipid layer was divided into two layers describing the tails and headgroups. The only parameter allowed to vary between the two SLD models was the SLD of the lipid tails. The thickness and SLD of the lipid layers were unconstrained to allow the possibility of insertion of protein segments. We did not assume that the amount of protein insertion into the lipid tails was the same for DPPG and d-DPPG. In fact, the data consistently

indicated slightly more insertion into the tails of d-DPPG. Initially we attempted to use a single layer in the SLD model to describe the protein layer, but in almost every instance two layers were required. Fitting reflectivity data always results in defining a family of SLD curves that are consistent with the data. The family of curves consistent with the data from two contrast conditions is a small subset of those that are consistent with the data from only a single contrast condition. Nevertheless, a range of acceptable values for each parameter still results. The range of uncertainty for any of the model parameters can be determined by fixing the value of that parameter in the fit and allowing the other parameters to vary within physically reasonable limits. In this work, upper and lower bounds were determined by the values that led to fits that were unacceptably poor, as indicated by an increase in χ^2 by a factor of 1.2. In the GAFIT program the roughness parameter corresponds to the full width at half-maximum ($= 2.35\ \sigma$, where σ is the standard deviation) of a Gaussian distribution. This parameter was constrained in the fitting to be less the smallest thickness of the two adjacent layers.

X-ray reflection and grazing incidence x-ray diffraction

XR and GIXD were performed on the liquid surface spectrometer on beamline ID-9 at the advanced photon source. The trough container was continuously purged with water-saturated helium to maintain an oxygen level <0.5% to minimize oxidative degradation of the organic monolayer in the presence of the intense x-ray beam and to reduce background scattering. Excellent reproducibility indicated the absence of beam damage. Analysis of the XR data was performed using the GAFIT program. First, the data for the lipid monolayers were analyzed using one layer for the headgroups and a second layer for the tails, where the thickness and electron density of the tails were constrained such that the number of electrons per unit area was fixed at the value calculated from the molecular structure and the known area per molecule at 30 mN/m. After addition of the protein, the constraint was relaxed to account for insertion of residues into this monolayer.

GIXD yields information on the lateral order within the surface structure (41). By monitoring the diffraction peak arising from the ordered packing of the lipid tails, the effect of protein binding and insertion on the structure and phase behavior of the lipid film can be examined. To maximize surface sensitivity for GIXD measurements, the monochromatic x-ray beam is adjusted to strike the surface at an incident grazing angle $\alpha_i \sim 0.1°$, which corresponds to the vertical momentum transfer vector $q_z = 0.85\ q_c$, where $q_c = 0.02176\ \text{Å}^{-1}$ is the critical scattering vector for total external reflection from a water surface. At this angle the incident wave is totally reflected from the sample, whereas the refracted wave becomes an evanescent wave traveling along the interface. The intensity of the evanescent wave decreases exponentially with depth, thus enhancing the surface sensitivity and reducing the background scattering from the subphase. The dimensions of the footprint of the incoming x-ray beam on the liquid surface were $\sim 2 \times 50\ \text{mm}^2$. For the collection of diffracted intensities, a vertical one-dimensional position-sensitive detector (PSD) with vertical acceptance $0 < q_z < 1.0\ \text{Å}^{-1}$ was used. A Soller collimator was mounted in front of the PSD, defining the horizontal resolution of the detector at $\Delta q_{xy} = 0.009\ \text{Å}^{-1}$. The scattered intensity was measured by scanning over a range of the horizontal scattering vector component,

$$q_{xy} = (q_x^2 + q_y^2)^{\frac{1}{2}}$$
$$= \frac{2\pi}{\lambda}[\cos^2(\alpha_i) + \cos^2(\alpha_f) - 2\cos(\alpha_i)\cos(\alpha_f)\cos(2\theta_{xy})]^{\frac{1}{2}}$$
$$\approx (4\pi/\lambda)\sin(2\theta_{xy}/2),$$

where $2\theta_{xy}$ is the angle between the incident and diffracted beam projected onto the horizontal plane, and q_{xy} is the combination of horizontal components q_x and q_y. Such a scan, integrated over all the channels along the q_z directions in the PSD, yields the Bragg peaks.

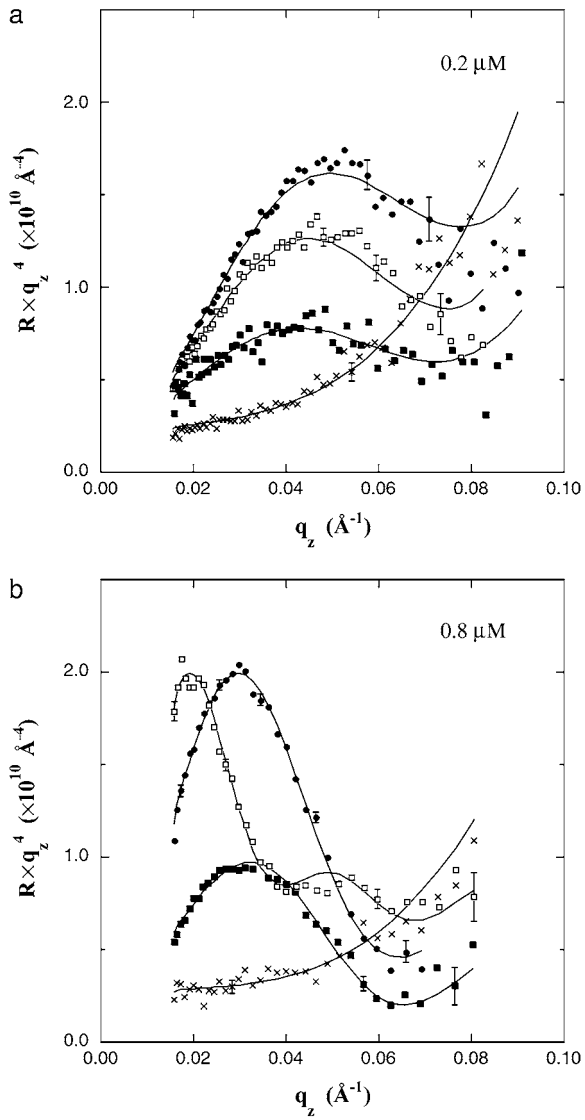

FIGURE 1 (*a*) Neutron reflectivity for an h-DPPG monolayer alone (x) and after injecting CRM197 at 0.2 μM and reducing the pH to 5.3 (■), 5.0 (□), and 4.5 (●). These data indicate increased occupancy but little change in the conformation. (*b*) Neutron reflectivity for an h-DPPG monolayer alone (x) and after injecting CRM197 at 0.8 μM and reducing the pH to 6.5 (■), 6.0 (●), and 5.4 (□). The increase in peak height from pH 6.5 to 6.0 indicates increased occupancy, whereas the change in the shape of the curve from pH 6.0 to 5.4 indicates a large change in the protein conformation.

RESULTS

NR data for CRM197 binding to Langmuir monolayers of h-DPPG are shown in Fig. 1 for bulk concentrations of 0.2 μM and 0.8 μM. At each concentration, NR data are shown as a function of pH. At 0.2 μM (Fig. 1 *a*), the data show only one broad peak over the accessible range of momentum transfer q_z, which reflects the total thickness of the surface layer (protein + lipid). With decreasing pH, the peak increased in magnitude, indicating an increase in occupancy, and shifted to slightly higher q_z, indicating a small decrease in the total

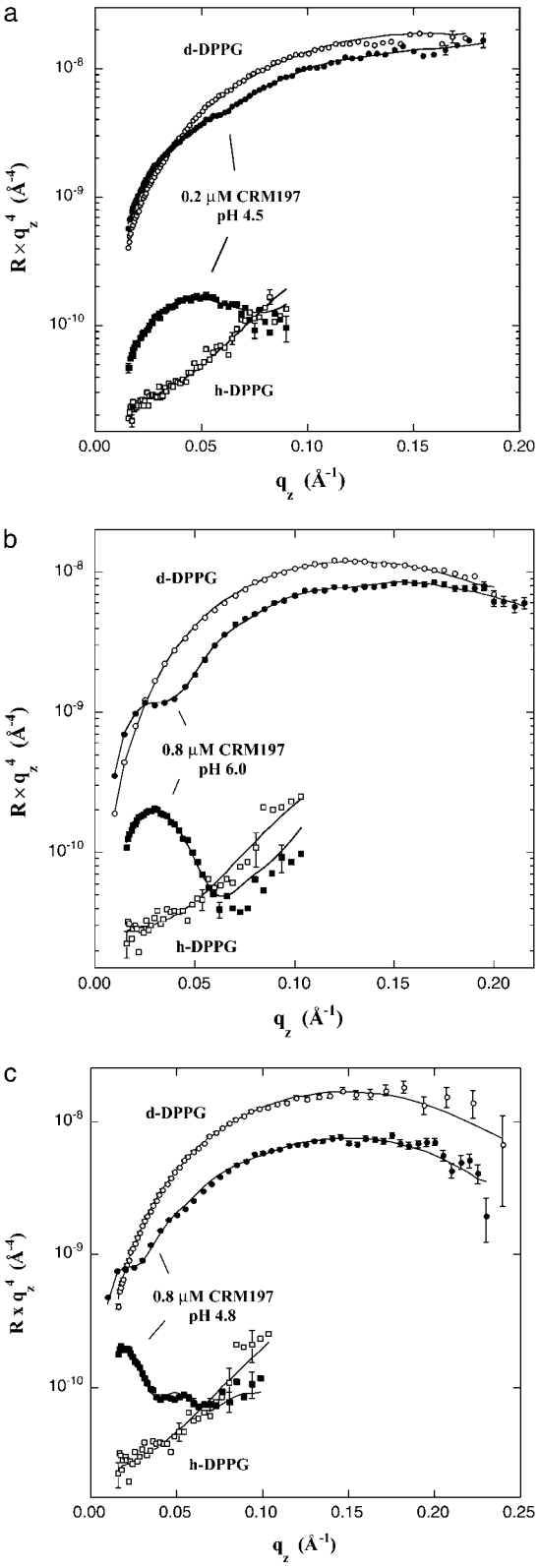

FIGURE 2 (*a*) Neutron reflectivity for h-DPPG (□) and d-DPPG (○) monolayers alone and after injecting DT at 0.2 μM and reducing the pH to 4.5 (■,●). The data for both contrast schemes were fit simultaneously to determine the SLD profile. (*b*) Neutron reflectivity for h-DPPG (□) and d-DPPG (○) monolayers alone and after injecting CRM197 at 0.8 μM and reducing the pH to 6.0 (■,●). (*c*) Neutron reflectivity for h-DPPG (□) and d-DPPG (○) monolayers alone and after injecting CRM197 at 0.8 μM and reducing the pH to 4.8 (■,●).

thickness. At 0.8 μM (Fig. 1 *b*), when adsorption was first detected (~pH 6.5), the peak occurred at lower q_z than at 0.2 μM ($q_z \sim 0.03$ compared to $q_z \sim 0.05$ at 0.2 μM), indicating a substantially thicker adsorbed structure. With further decrease in pH, the peak first increased in magnitude at the same q_z value, indicating a constant conformation but higher occupancy, and then shifted strongly to lower q_z. The shift to lower q_z is a critical insight from NR, as it indicates a surprising elongation of the adsorbed protein. The shift was first observed to occur at pH 5.4. The peak continued to shift to lower q_z and to increase slightly in magnitude with further decrease in pH (see Supplementary Fig. 1).

Detailed analysis of NR data is greatly facilitated by performing identical measurements in different contrast conditions. Simultaneously fitting data for two contrast conditions severely restricts the range of profile characteristics that are compatible with the data. To that end, NR data were also acquired for the same conditions as in Fig. 1 but using DPPG with fully deuterated aliphatic tails (d-DPPG). Examples are provided in Fig. 2. With d-DPPG the reflectivity is substantially increased, allowing data to be obtained to higher q_z values. However, the sensitivity to the adsorbed protein is much greater with h-DPPG. Simultaneously fitting the two data sets combines the benefits of the two contrast schemes. Parameters from a simultaneous fitting analysis in which only the SLD of the lipid tail layer varies between the two contrast conditions are given in Table 1.

SLD profiles for 0.2 μM CRM197 are shown in Fig. 3 *a* for both contrast conditions at pH 4.5 and in Fig. 3 *b* for h-DPPG at several pH values. In each plot the SLD profile for the lipid monolayer alone is included for comparison. The profiles show that very little change in the structure of the adsorbed protein occurs with decreasing pH. This has several important implications. It indicates that for pH values down to 4.5 large conformational change of the T domain does not occur, the C domain does not unfold, and oligomerization normal to the surface does not occur. The inner and outer protein layers likely correspond to the C + T and R domains, respectively. This should be definitively resolved in future work with CRM197 in which one domain is enriched in deuterium. A χ^2 analysis for the total thickness of the surface layer (DPPG + protein) yields a range from 80 Å to 96 Å (corresponding to an increase in χ^2 by a factor of 1.2). The plot is provided in Supplementary Fig. 2.

SLD profiles for 0.8 μM are shown in Fig. 4 *a* for both contrast conditions at pH 4.8 and in Fig. 4 *b* for h-DPPG at several pH values. In contrast to the results at 0.2 μM, at 0.8 μM large changes occur with decreasing pH. From pH 6.5 to pH 6.0 the thickness is nearly constant as the occupancy increases. For pH values below 6.0, there is a large increase in the thickness of the adsorbed structure as well as further

TABLE 1 Fitting parameters from combined analysis of NR data with d-DPPG and h-DPPG

Layer	SLD ($\times 10^6$ Å^{-2})	Thickness (Å)	Roughness (Å)*
(DPPG)			
Lipid tails (d-DPPG)	5.77	16	3
Lipid tails (h-DPPG)	−0.25	16	3
Lipid heads	1.64	7	3
Subphase	−0.40		3
(0.2 μM CRM197, pH 5.3)			
Lipid tails (d-DPPG)	5.77	15	3
Lipid tails (h-DPPG)	−0.25	15	3
Lipid heads	1.64	9	3
CRM197, inner	−0.063	33	7
CRM197, outer	−0.17	30	6
Subphase	−0.40		15
(0.2 μM CRM197, pH 5.0)			
Lipid tails (d-DPPG)	5.77	15	3
Lipid tails (h-DPPG)	−0.25	15	3
Lipid heads	1.36	9	3
CRM197, inner	0.25	27	4
CRM197, outer	−0.058	35	20
Subphase	−0.40		20
(0.2 μM CRM197, pH 4.5)			
Lipid tails (d-DPPG)	5.77	15	3
Lipid tails (h-DPPG)	−0.25	15	3
Lipid heads	1.34	8	3
DT, inner	0.40	24	7
DT, outer	−0.034	37	16
Subphase	−0.40		20
(DPPG)			
Lipid tails (d-DPPG)	5.60	16	3
Lipid tails (h-DPPG)	−0.43	16	3
Lipid heads	1.50	9	3
Subphase	−0.45		3
(0.8 μM CRM197, pH 6.5)			
Lipid tails (d-DPPG)†	4.09	19	3
Lipid tails (h-DPPG)†	−0.23	19	3
Lipid heads†	0.86	11	3
CRM197, inner	0.18	61	3
CRM197, outer	−0.20	36	20
Subphase	−0.45		25
(0.8 μM CRM197, pH 6.0)			
Lipid tails (d-DPPG)†	3.98	21	3
Lipid tails (h-DPPG)†	−0.094	21	3
Lipid heads†	0.518	27	3
CRM197, inner	0.43	49	3
CRM197, outer	−0.11	44	25
Subphase	−0.45		25
(0.8 μM CRM197, pH 5.4)			
Lipid tails (d-DPPG)†	3.87	21	3
Lipid tails (h-DPPG)†	0.020	21	3
Lipid heads†	0.63	26	3
CRM197, inner	0.50	60	5
CRM197, outer	−0.11	68	60
Subphase	−0.45		60
(0.8 μM CRM197, pH 4.8)			
Lipid tails (d-DPPG)†	3.79	21	3
Lipid tails (h-DPPG)†	0.032	21	3
Lipid heads†	0.65	68	3
CRM197, inner	0.16	67	60
CRM197, outer	−0.23	60	50
Subphase	−0.45		60

*Values reported are full width at half-maximum = 2.35 σ, where σ is the standard deviation of a Gaussian distribution.
†Contains protein segments as well.

increased occupancy. The former is indicated by the shift in the peak position to lower q_z in Fig. 1 *b*. A χ^2 analysis for the total thickness of the surface layer (DPPG + protein) yields a range from 136 Å to 150 Å for 0.8 μM at pH 6.0 and a range from 193 Å to 244 Å for 0.8 μM at pH 4.8. The plots are provided in Supplementary Fig. 2. The SLD profiles also reveal strong insertion of residues into the lipid tail region at the lower pH values, discussed further below, simultaneous with the extension into the subphase.

SLD profiles for 0.2 μM at pH 4.5 and for 0.8 μM at pH 6.0 (before the pH-driven conformational change) are compared in Fig. 5. The data for both contrast conditions (h-DPPG and d-DPPG) were fit simultaneously, but Fig. 5 shows only the profiles for h-DPPG for clarity. The thickness ranges for the two cases mentioned above are consistent with the dimensions of the crystal structures for monomeric DT (1F0L) (13) and dimeric DT (1DDT) (14,23), respectively, in the orientations roughly depicted in the insets in Figs. 3 *b* and 4 *b*. A detailed comparison of the data with SLD profiles for a set of likely orientations of the crystal structures will be reported elsewhere. However, one example of volume fraction profiles for the monomeric and dimeric forms (protein only) is given in the inset to Fig. 5 to show the general correspondence of the thicknesses with those of the measured SLD profiles. The difference in thickness upon first adsorption for 0.2 μM and 0.8 μM implies that an increase in bulk concentration drives a transition in the adsorbed protein from a monomeric state to a dimeric state normal to the plane of the membrane. We note that in bulk solution the protein remains monomeric over the same range of concentration and pH, as shown by native gel electrophoresis (see Supplementary Fig. 3), indicating that oligomerization occurs only for the membrane-bound toxin. From integration of the SLD profiles in Fig. 5, the surface occupancy is ~34% of a full monolayer of monomeric DT at 0.2 μM and pH 4.5 and ~40% of a full monolayer of dimeric DT at 0.8 μM and pH 6.0.

Regarding the extension of the profile with decreasing pH at 0.8 μM, we propose that in the oligomeric state a transition occurs from the closed to the open form with decreasing pH, as illustrated in the inset in Fig. 4 *b*. (Although the R domain-swapped dimeric state has sometimes been referred to as the ''open'' state since the R domains are extended from the C and T domains relative to their positions in the

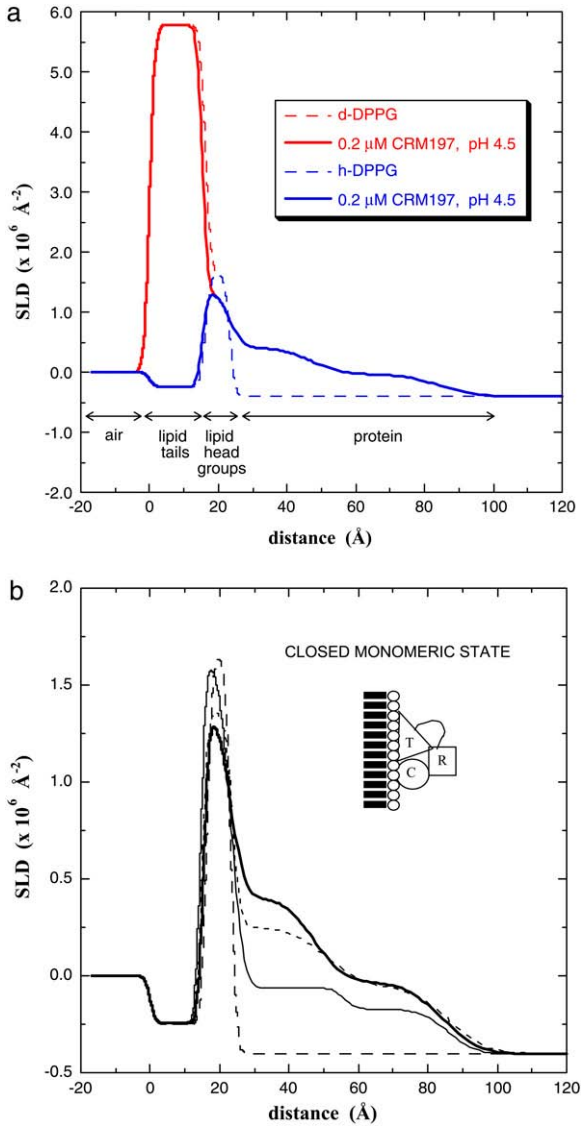

FIGURE 3 SLD profiles for 0.2 μM CRM197. (*a*) Profiles for d-DPPG (*red line*) and h-DPPG (*blue line*) in the absence of CRM197 (*dashed lines*) and after injecting CRM197 at 0.2 μM and lowering the pH to 4.5 (*solid lines*). (*b*) Profiles for h-DPPG in the absence of CRM197 (*dashed line*) and after injecting CRM197 at 0.2 μM and lowering the pH to 5.3 (*thin solid line*), 5.0 (*dotted line*), and 4.5 (*thick solid line*). The profiles reveal that little conformational change occurs in CRM197 upon lowering the pH at this bulk concentration. At pH 4.5, the occupancy is ~34% of a full monolayer of monomeric DT.

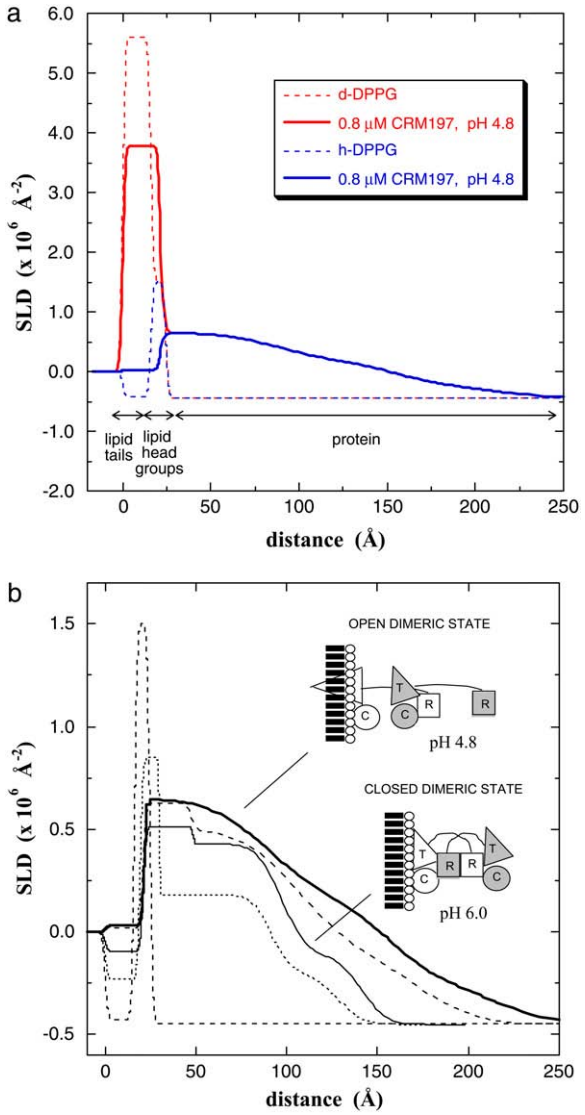

FIGURE 4 SLD profiles for 0.8 μM CRM197. (*a*) Profiles for d-DPPG (*red lines*) and h-DPPG (*blue lines*) in the absence of CRM197 (*dashed lines*) and after injecting CRM197 at 0.8 μM and lowering the pH to 4.8 (*solid lines*). (*b*) Profiles for h-DPPG in the absence of CRM197 (*dashed line*) and after injecting CRM197 at 0.8 μM and lowering the pH to 6.5 (*dotted line*), 6.0 (*thin solid line*), 5.4 (*thick dashed line*), and 4.8 (*thick solid line*). The profiles reveal that, for the dimeric state, CRM197 extends into the subphase and penetrates into the lipid tails upon decrease in pH. At pH 4.8, the occupancy is ~40% of a full monolayer of dimeric DT.

monomeric state, hereafter we use the term ''open'' for the further extension of the structure upon decrease in pH following Steere and Eisenberg (23)).

As mentioned in the Introduction, an important aspect of the adsorbed protein structure is the extent of insertion of segments into the hydrophobic lipid tails. This was quantified as follows. For the data with DPPG alone, the thickness of the tail layer was constrained to the value obtained from XR $\pm$ 1.5 Å. After the addition of CRM197, the data were modeled with two layers for DPPG (headgroups and tails) and two layers for the protein (after it was determined that a single layer for the protein was not sufficient). Initially these four layers were unconstrained. To determine the extent of insertion in each case, the SLD of the lipid tail layer was fixed at various values in the fits while allowing the other parameters to vary within physically realistic limits. The amounts of protein insertion into h-DPPG and d-DPPG were not constrained to the same value to allow for a possible effect of deuteration. The χ^2 analysis for the SLD of the tail layer was much more sensitive for d-DPPG than for h-DPPG,

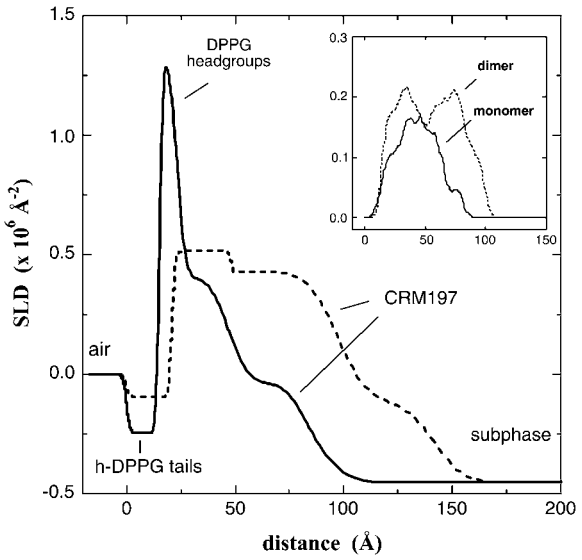

FIGURE 5 SLD profiles for adsorbed CRM197 at 0.2 μM and pH 4.5 (*solid line*) and at 0.8 μM and pH 6.0 (*dashed line*). The SLD profiles were derived from simultaneous fitting of the data in Fig. 2, *a* and *b*. These profiles are consistent with predominantly monomeric CRM197 at 0.2 μM and mostly dimeric CRM197 at 0.8 μM, illustrated by the diagrams in Figs. 3 *b* and 4 *b*. The inset shows calculated volume fraction profiles from crystal structure data for DT in monomeric (1F0L) and dimeric (1DDT) states in the orientations indicated in the diagrams.

due to the much higher range of q_z in that case. Plots of χ^2 versus tail layer SLD are given in Supplementary Fig. 4 for 0.8 μM CRM197 at pH 4.8 and for 0.2 μM CRM197 at pH 4.5. The analysis yields a range for SLD_{tails} from 3.71×10^{-6} Å^{-2} to 3.96×10^{-6} Å^{-2} for 0.8 μM CRM197 at pH 4.8 (increase in χ^2 by 1.2), whereas the value in the absence of CRM197 is 5.6×10^{-6} Å^{-2}. This decrease in SLD in the tail layer after insertion of CRM197 corresponds to a protein segment volume fraction in the lipid tails ranging from 0.45 to 0.53. At 0.2 μM CRM197, the χ^2 analysis yields a range of SLD_{tails} from 4.6×10^{-6} Å^{-2} to 6.8×10^{-6} Å^{-2}, whereas the value in the absence of CRM197 is 5.9×10^{-6} Å^{-2}. Therefore, the data are consistent with little or no insertion at 0.2 μM CRM197 and pH 4.5. Based on this result and on the absence of a significant increase in the area per molecule upon introducing CRM197 at 0.2 μM as described below, the parameters reported in Table 1 at 0.2 μM were determined for fits in which the parameters of the tail layers were held constant at the values obtained in the absence of CRM197, allowing for a 5% decrease in thickness as suggested by a small increase in the area (discussed below).

NR data (h-DPPG only) were also obtained at 0.1 μM and 0.93 μM CRM197. The data for several pH values in each case are shown in Fig. 6, *a* and *b*. These data show the same trends with pH and solution concentration as the data for 0.2 μM and 0.8 μM in Fig. 1. Since NR data were obtained in this case only with h-DPPG (and not with d-DPPG), the extent of insertion into the lipid tails, and thus the full SLD profiles, could not be determined. However, the peak positions indicate that the overall thicknesses and the changes in thickness with pH are similar for 0.1 μM and 0.2 μM and for 0.8 μM and 0.93 μM. At 0.93 μM, NR data were collected for a large number of pH values. This revealed that the changes in conformation were not continuous with pH, but rather stronger and weaker change occurred over different pH ranges. In particular, little change in the NR data occurred from pH 6.0 to pH 5.8, from pH 5.5 to pH 5.3, or from pH 4.8 to pH 4.5. This is shown in Fig. 6 *c*. In each case, reflectivity scans were performed until little change was observed in the reflectivity with time, such that the system was maintained at each pH value for a minimum of 6 h. These data suggest that the transition, which we interpret as from the closed to the open form, occurs in stages with decreasing pH. Estimates of the adsorbed amounts at 0.1 μM and 0.93 μM from analysis of the data for h-DPPG alone are plotted in Fig. 7 along with the values obtained at 0.2 μM and 0.8 μM. A consistent trend in all our data is that the pH value at which adsorption first becomes detectable increases with increasing bulk concentration.

Details of the protein-lipid interaction were also revealed by changes in the surface area of the Langmuir monolayers, which were maintained at constant surface pressure such that insertion of protein segments into the lipid films resulted in increases in total area. The fractional changes in area as a function of pH for 0.2 μM and 0.8 μM are shown in Fig. 8. Little change in area was observed at 0.2 μM for pH values down to 4.5, whereas a large increase in area with decreasing pH resulted at 0.8 μM. Specifically, at 0.8 μM the area increased ~10% at pH 6.0, followed by a much greater increase upon lowering the pH to 5.4. Importantly, this is the pH value at which the shift in the peak in the NR data occurred in Fig. 1 *b*. Thus the changes in surface area confirm that the extension of the profile into the subphase at 0.8 μM coincides with insertion of residues into the lipid tails, supporting the conclusion from the SLD profiles in Fig. 4. After lowering the pH to 5.4 at 0.8 μM, the area increased until the barrier reached the back of the trough. After collecting reflectivity at this condition, additional citric acid was introduced to lower the pH to 4.8 for the final NR scans, this time at fixed area. At this point an increase in surface pressure of a few mN/m resulted. The magnitude of the area increase at pH 5.4 (~60%) is reasonably consistent with the volume fraction of protein segments within the tail layer determined from the NR data at pH 5.4 and pH 4.8 (45–53%).

Further corroborating evidence for strong insertion of residues into the lipid tails with decreasing pH exclusively at the higher concentration range was obtained with GIXD (Fig. 9) and XR (Fig. 10). Fig. 9 *a* shows Bragg peaks from GIXD for an h-DPPG monolayer alone at 30 mN/m and after injecting CRM197 at 0.3 μM and reducing the pH to 5.3, 4.9, and 4.2. The two peaks arise from the distorted hexagonal lattice of the DPPG tails in the gel phase (42). The peaks are relatively unchanged after injecting CRM197

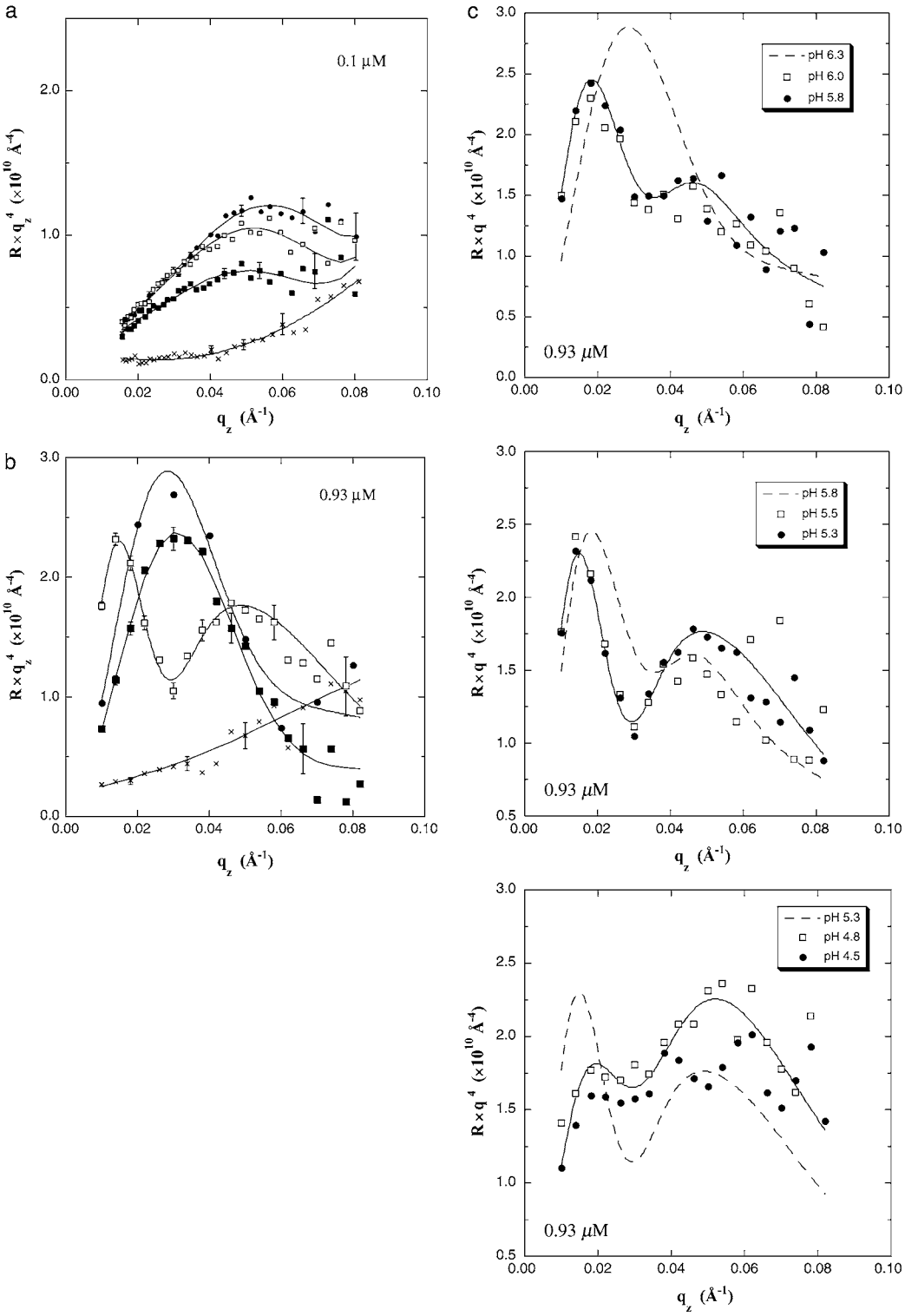

FIGURE 6 (*a*) Neutron reflectivity for an h-DPPG monolayer alone (x) and after injecting CRM197 at 0.1 μM and reducing the pH to 5.1 (■), 4.7 (□), and 4.0 (●). These data indicate increased occupancy but little change in CRM197 conformation. (*b*) Neutron reflectivity for an h-DPPG monolayer alone (x) and after injecting CRM197 at 0.93 μM and reducing the pH to 6.5 (■), 6.3 (●), and 5.3 (□). The increase in peak height from pH 6.5 to 6.3 indicates increased occupancy, whereas the change in the shape of the curve from pH 6.3 to 5.3 indicates a large change in protein conformation. (*c*) NR data for h-DPPG monolayers incubated with 0.93 μM DT CRM197 at various pH values, demonstrating regimes of strong and weak pH dependence. (*top panel*) NR data for CRM197/h-DPPG at pH 6.3, pH 6.0, and pH 5.8. The data at pH 6.3 are represented as a dashed line. Little change occurs over the pH range 6.0–5.8. (*middle panel*) NR data for CRM197/h-DPPG at 5.8, pH 5.5, and pH 5.3. The data at pH 5.8 are represented as a dashed line. Little change occurs over the pH range 5.5–5.3. (*bottom panel*) NR data for CRM197/h-DPPG at pH 5.3, pH 4.9, and pH 4.5. The data at pH 5.3 are represented as a dashed line. Little change occurs over the pH range 4.9–4.5.

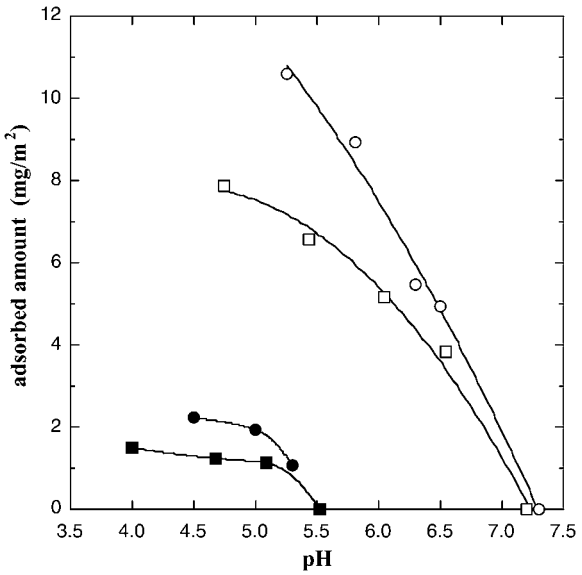

FIGURE 7 Adsorbed amount versus pH for CRM197 at 0.1 μM (■), 0.2 μM (●), 0.8 μM (□), and 0.93 μM (○).

at 0.3 μM and lowering the pH to 4.2, indicating little or no insertion of CRM197 into the tails. In contrast, Fig. 9 *b* shows that at 0.93 μM CRM197 the Bragg peaks for the DPPG monolayer were substantially reduced at pH 5.7 and were completely absent at pH 5.1. This indicates strong insertion of CRM197 into the lipid tails at pH 5.1, such that the liquid crystalline order was completely disrupted. Fig. 10 *a* shows corresponding XR data for a h-DPPG monolayer alone at 30 mN/m and after injecting CRM197 at 0.3 μM and reducing the pH to 4.2. The sharp fringes indicate a laterally uniform lipid film and arise from the elevated electron density of the DPPG headgroups and the total length of the lipid molecule. The fringes were relatively unchanged after injecting CRM197 at 0.3 μM and lowering the pH to 4.2, indicating little or no insertion of CRM197 into the lipid layer. In contrast, Fig. 10 *b* shows XR data for a h-DPPG monolayer alone and after injecting DT at 0.93 μM and reducing the pH to 5.7 and 5.1. The decrease in the magnitude of the fringes upon lowering the pH indicates strong insertion of CRM197 into the DPPG film. In addition to being highly sensitive to insertion of segments into the lipid monolayer, XR is sensitive to the details of the adsorbed protein layer, although less so than NR. The characteristics of the adsorbed protein layer affect the XR data in the low q_z region, shown in an expanded view in Fig. 10, *c* and *d*. Parameters from the fitting analysis are given in Table 2. Best-fit electron density profiles are given in Fig. 11 (note the change in scale of the *x* axis). At 0.3 μM the effect of adsorbed CRM197 on the XR curve is weak, and only the dense layer of protein segments at the interface with the lipid could be resolved. At 0.93 μM several layers were required for the protein in the model profile, and the thicknesses are reasonably consistent with the NR results at 0.8 μM in Fig. 4.

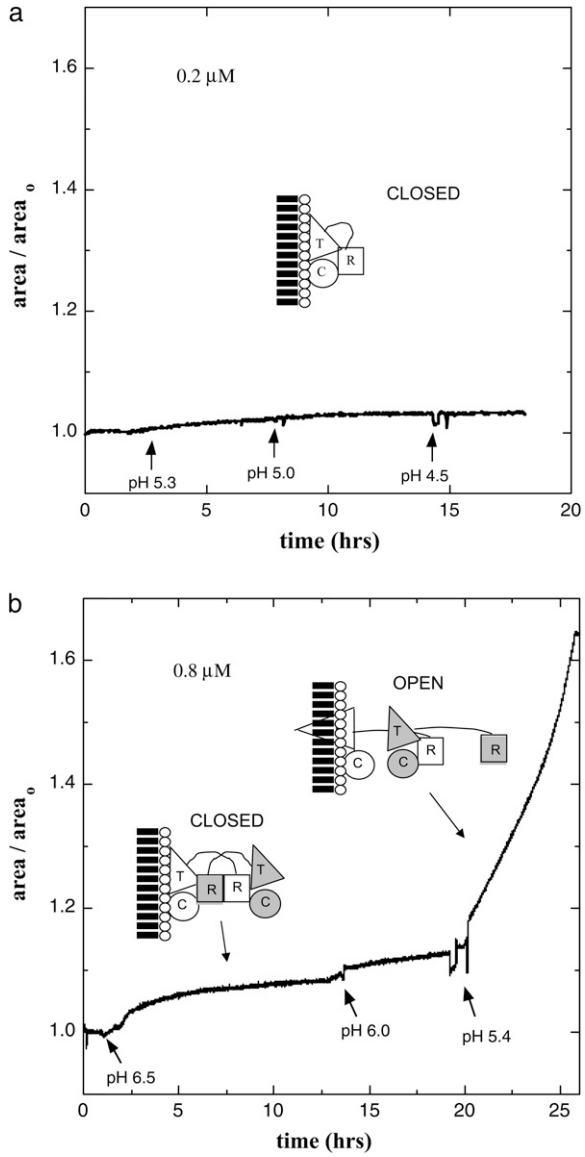

FIGURE 8 Fractional change in area after addition of CRM197 and lowering the pH for CRM197 concentrations of 0.2 μM (*a*) and 0.8 μM (*b*). The sharp increase in area in the latter case indicates a strong insertion of segments into the lipid film at pH 5.4 where the profile extension was first observed by NR. The arrows indicate injections of citric acid and the corresponding pH values.

DISCUSSION

This work has several important implications for the interaction of DT with lipid membranes and the translocation process. Our data show for the first time, to our knowledge, that large changes in the conformation of membrane-bound DT occur normal to the plane of the membrane, both in the formation of oligomers and in the extension/insertion transition that the oligomeric form undergoes with decreasing pH. Previous evidence for oligomerization has been reported for DT interacting with lipid vesicles over a similar

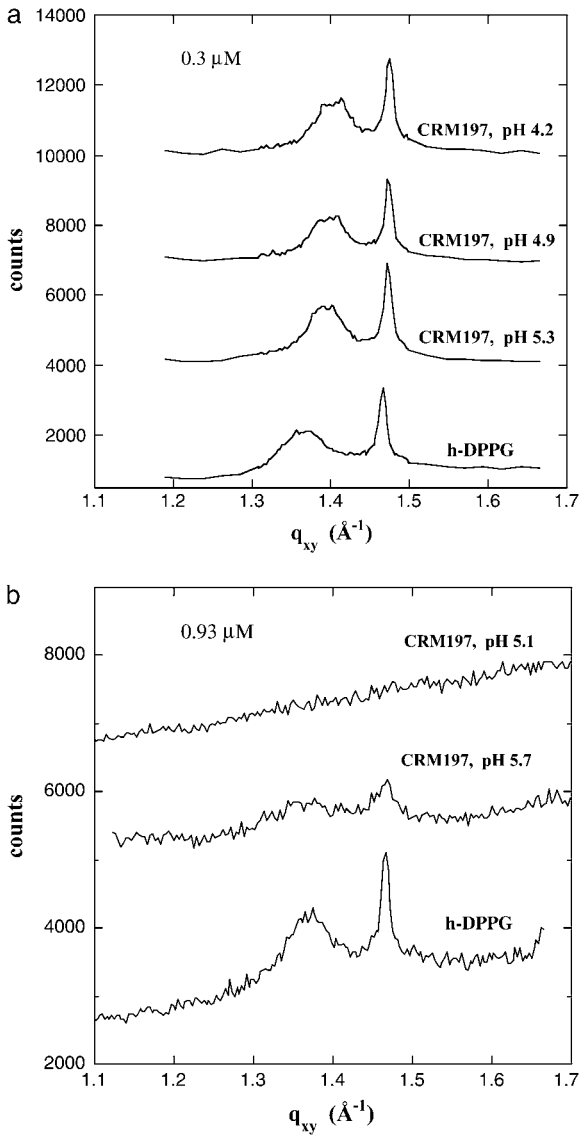

FIGURE 9 (*a*) Bragg peaks from grazing incidence x-ray diffraction (GIXD) for a h-DPPG monolayer alone at 30 mN/m and after injecting CRM197 at 0.3 μM and reducing the pH to 5.3, 4.9, and 4.2. The two peaks arise from the distorted hexagonal lattice of the DPPG tails in the gel phase. The peaks were relatively unchanged after injecting CRM197 at 0.3 μM and lowering the pH to 4.2, indicating little or no insertion of protein segments into the tails and preservation of the alkyl tail in-plane ordering. (*b*) Bragg peaks for a h-DPPG monolayer alone and after injecting CRM197 at 0.93 μM and reducing the pH to 5.7 and 5.1. The absence of the peaks after injecting CRM197 and lowering the pH to 5.1 indicates disruption of the in-plane order, suggesting strong insertion of protein segments into the DPPG monolayer.

concentration range as in this study (25). In that work, liposome leakage studies suggested a pore whose size depended upon DT concentration. However, the nature of the structure was not revealed, and the discussion considered only lateral assembly. Indeed, several bacterial toxins such as α hemolysin and anthrax are known to associate laterally to form pores (43,44). Our data indicate a more complex assembly for DT that includes dimerization and conformational changes normal to the membrane. The above-mentioned study reported release of fairly large molecules that would seem to require a pore composed of more than a single DT molecule (25). Lateral assembly may indeed have occurred in the present system in addition to the changes normal to the membrane. Such lateral assembly would be undetectable by specular reflection. Because of that possibility, we refer to the structure as oligomeric despite the fact that the reflectivity data reveal a dimeric dimension normal to the membrane.

Our results strongly suggest that as a function of bulk DT concentration, adsorbed DT passes from an inactive monomeric state to an active oligomeric state. Further, the data suggest that in the oligomeric state, a transition to the open form coincides with insertion of residues into the hydrophobic lipid tails. We propose that in monomeric DT interactions between the R and T domains hold the conformation in the closed form, but in the dimeric state the intramolecular interactions are weakened, which allows the structure to pass to the open form with decreasing pH, as discussed previously by Steere and Eisenberg (23). Thus, our data imply that only in the open form is the T domain free to insert. Here the open form was enabled by oligomerization over a range of bulk concentration from 0.2 μM to 0.8 μM. The actual concentration of DT in endosomes is not well known. However, in studies involving translocation of C directly across the plasma membrane, Olsnes et al. have shown pH-driven translocation at a bulk DT concentration of 1 nM (28,29), far lower than the range of the oligomerization observed here. In this work CRM197 adsorbed directly to the negatively charged lipid membrane in the absence of the HB-EGF receptor. The binding of R to the receptor occurs with much higher affinity (10^{-8}–10^{-9} M) (45), resulting in the activity of the toxin at much lower concentrations. Previous work has shown that the binding of monomeric DT to the receptor may actually promote dimerization (15). Together with the results here, this suggests that dimerization may indeed be the activating step at much lower concentration in the presence of the receptor. However, confirmation of this awaits further studies.

Finally, in other work that may be related, Wang et al. studying the T domain alone reported a transition from shallow to deep insertion as a function of the concentration of T within the membrane (20). This suggests that membrane-bound T associates above a critical concentration in the membrane and that association of T is somehow related to deep insertion. Our results with the full toxin show that a transition to deep insertion occurs only for the oligomeric form and coincides with a large extension of the structure into the subphase that we interpret as a transition to the open form. Thus, it may be that with the full toxin the lateral association of the T domains occurs only in the open form. It is tempting to speculate that dimerization and the transition to the open form trigger both lateral association of T and insertion. However, more work is needed to test this hypothesis.

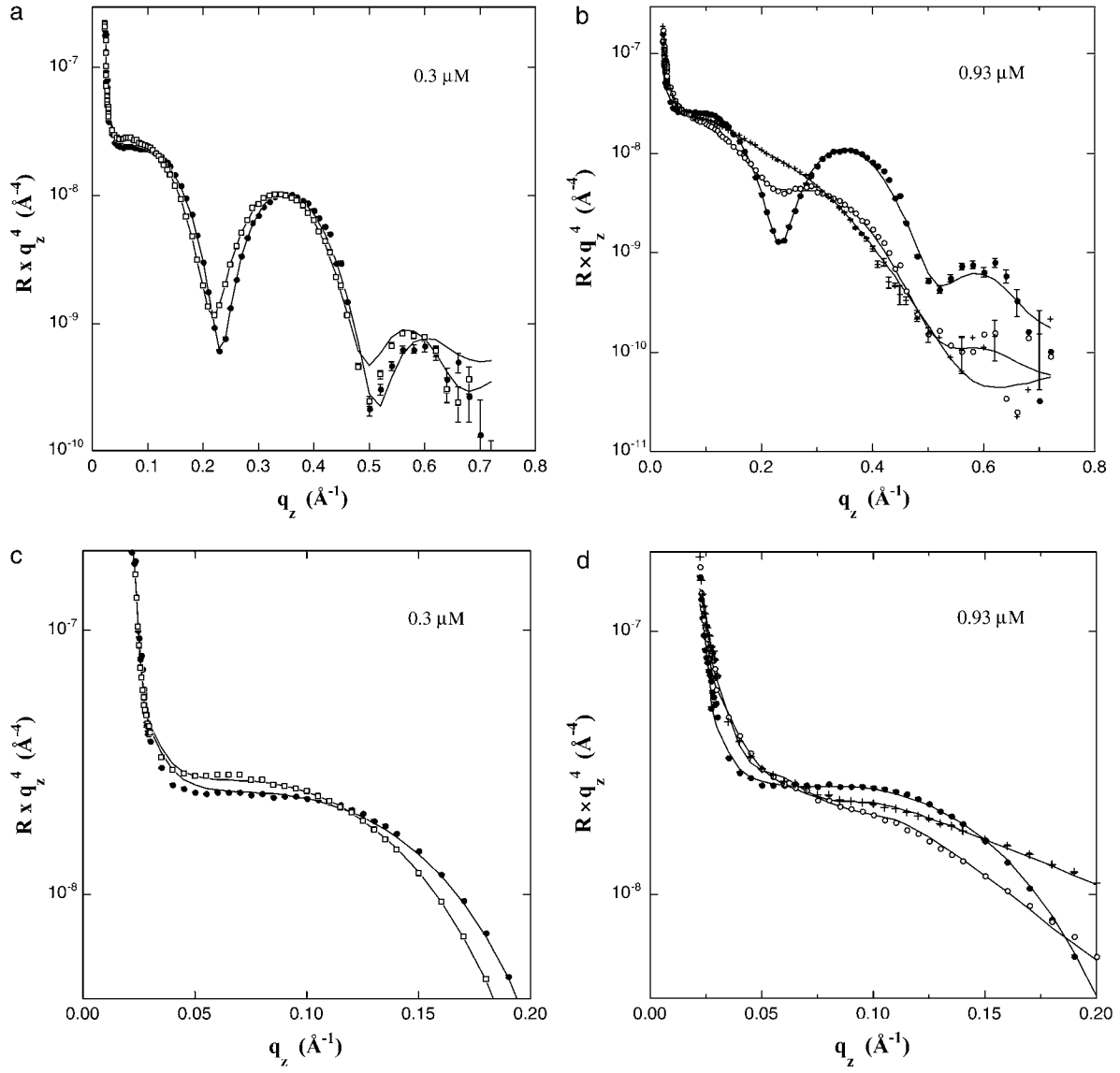

FIGURE 10 (*a*) XR for a h-DPPG monolayer alone at 30 mN/m (●) and after injecting CRM197 at 0.3 μM and reducing the pH to 4.2 (□). The sharp fringes indicate a laterally uniform film and arise from the elevated electron density of the DPPG headgroups and the total length of the molecule. The fringes were relatively unchanged after injecting CRM197 at 0.3 μM and lowering the pH to 4.2, indicating little or no insertion of protein into the DPPG monolayer. (*b*). XR for a h-DPPG monolayer alone (●) and after injecting CRM197 at 0.93 μM and reducing the pH to 5.7 (○) and 5.1 (+). The absence of the fringes after injecting CRM197 at 0.93 μM and lowering the pH to 5.1 indicates strong insertion of protein segments into the DPPG monolayer. (*c*) Expanded view of the low q_z region of the data in *a*. (*d*) Expanded view of the low q_z region of the data in *b*.

In summary, NR has revealed that membrane-bound CRM197 oligomerizes as a function of bulk concentration and that with decreasing pH the oligomeric form undergoes a significant extension normal to the surface that coincides with deep insertion. The oligomeric structure has a dimeric dimension normal to the plane of the membrane. We anticipate that further NR studies in which the HB-EGF receptor is incorporated into the lipid membrane and where individual domains of the toxin are enriched in deuterium will elucidate further details of this process. The model system in this study is intended to mimic the process of protein-membrane binding and pH-dependent conformational change that occurs within endosomes. However, we note that our model system has a number of deficiencies with respect to cellular membranes. In particular, the membrane composition of 100% DPPG, chosen in this initial study to reduce the amount of protein required, is not representative of a real cell membrane. In the case here the very strong electrostatic interactions likely result in an elevated proton concentration near the membrane, and membrane-bound protein residues may protonate at a higher pH that would otherwise be the case. Future work will explore the effect of varying the percentage of charged and neutral lipids. Also important is to examine the effect of the lipid phase state by obtaining

TABLE 2 Fitting parameters from analysis of XR data

Layer	$\rho_e/\rho_{e\ sub}$ ($\times 10^6$ Å^{-2})	Thickness (Å)	Roughness (Å)*
(h-DPPG)			
Lipid tails	0.91	15.2	8.6
Lipid heads	1.25	11.0	7.0
Subphase	1.0		2.6
(0.3 μM CRM197, pH 4.2)			
Lipid tails	0.91	15.6	8.1
Lipid heads	1.26	11.8	7.0
CRM197	1.05	10.5	2.9
Subphase	1.0		7.0
(h-DPPG)			
Lipid tails	0.94	15.2	8.1
Lipid heads	1.27	11.2	7.0
Subphase	1.0		4.4
(0.93 μM CRM197, pH 5.7)			
Lipid tails1†	0.87	7.6	8.7
Lipid tails2†	1.08	11.4	9.2
Lipid heads†	1.24	7.1	6.4
CRM197, inner	1.10	59.6	16.3
CRM197, outer	1.04	52.8	40.0
Subphase	1.00		40.0
(0.93 μM CRM197, pH 5.1)			
Lipid tails1†	1.06	7.3	9.4
Lipid heads†	1.14	23.6	7.0
CRM197, inner	1.10	53.2	13.2
CRM197, outer	1.06	80.0	35.3
Subphase	1.00		60.0

*Values reported are full width at half-maximum = 2.35 σ, where σ is the standard deviation of a Gaussian distribution.
†Contains protein segments as well.

results for lipids in the fluid phase for comparison with these results involving lipids in the gel phase. In addition, Langmuir monolayers at best mimic only one leaflet of a bilayer. Thus the membrane-inserted conformation will not be identical to that occurring in a cell. Ongoing work involving supported lipid bilayers will examine inserted DT in a configuration more similar to that in cells. Finally, studies that probe the in-plane structure of the adsorbed protein will be important to complement the reflectivity data and determine the overall oligomeric structure.

SUPPLEMENTARY MATERIAL

To view all of the supplemental files associated with this article, visit www.biophysj.org.

We thank Frank Heinrich and Mathias Loesche for use of the script to calculate volume fraction profiles from crystal structure coordinates. Sandia is a multi-program laboratory operated by Sandia Corporation, a Lockheed Martin Company, for the U.S. Department of Energy under contract DE-AC04-94AL85000.

We acknowledge the support of the National Institute of Standards and Technology, U.S. Department of Commerce, and the Los Alamos Neutron Science Center at the Los Alamos National Laboratory in providing the neutron research facilities used in this work. The latter facility is funded by the U.S. Department of Energy under Contract W-7405-ENG-36. Use of the Advanced Photon Source (CMC-CAT) was supported by the U.S. Department of Energy, Office of Basic Energy Sciences, under Contract No. W-31-109-Eng-38.

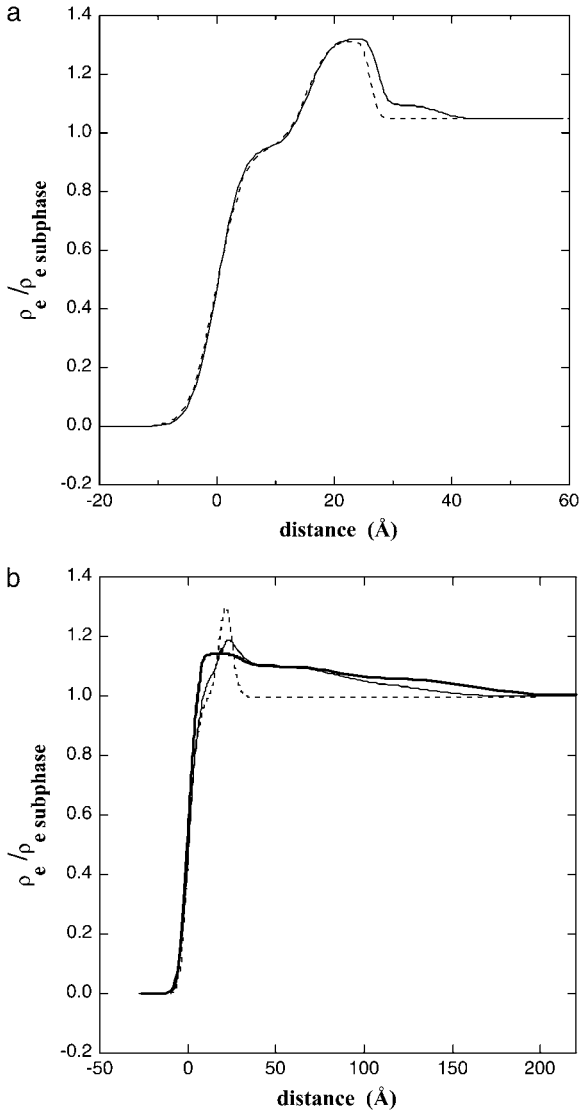

FIGURE 11 Normalized electron density profiles for h-DPPG alone (*dashed lines*) and (*a*) with CRM197 at 0.3 μM and pH 4.2 (*solid line*) and (*b*) with CRM197 at 0.93 μM and pH 5.7 (*thin solid line*) and pH 5.1 (*thick solid line*).

REFERENCES

1. Chenal, A., P. Nizard, and D. Gillet. 2002. Structure and function of diphtheria toxin: from pathology to engineering. *J. Toxicol. Toxin Rev.* 21:321–358.
2. Collier, R. 2001. Understanding the mode of action of diphtheria toxin: a perspective on progress during the 20th century. *Toxicon.* 39:1793–1803.
3. Sandvig, K., and B. van Deurs. 2002. Membrane traffic exploited by protein toxins. *Annu. Rev. Cell Dev. Biol.* 18:1–24.
4. Madshus, I. H., and H. Stenmark. 1992. Entry of ADP-ribosylating toxins into cells. *Curr. Top. Microbiol. Immunol.* 175:1–26.
5. Pappenheimer, A. M. Jr. 1977. Diphtheria toxin. *Annu. Rev. Biochem.* 46:69–94.
6. Klingenberg, O., and S. Olsnes. 1996. Ability of methotrexate to inhibit translocation to the cytosol of dihydrofolate reductase fused to diphtheria toxin. *Biochem. J.* 313:647–653.
7. Wiedlocha, A., I. H. Madshus, H. Mach, C. R. Middaugh, and S. Olsnes. 1992. Tight folding of acidic fibroblast growth factor prevents

its translocation to the cytosol with diphtheria toxin as vector. *EMBO J.* 11:4835–4842.

8. Sundan, A., S. Olsnes, K. Sandvig, and A. Pihl. 1982. Preparation and properties of chimeric toxins prepared from the constituent polypeptides of diphtheria toxin and ricin. Evidence for entry of ricin A-chain via the diphtheria toxin pathway. *J. Biol. Chem.* 257:9733–9739.
9. Francis, J. W., R. H. Brown Jr., D. Figueiredo, M. P. Remington, O. Castillo, M. A. Schwarzschild, P. S. Fishman, J. R. Murphy, and J. C. vanderSpek. 2000. Enhancement of diphtheria toxin potency by replacement of the receptor binding domain with tetanus toxin C-fragment: a potential vector for delivering heterologous proteins to neurons. *J. Neurochem.* 74:2528–2536.
10. Francis, J. W., D. Figueiredo, J. C. vanderSpek, L. M. Ayala, Y. S. Kim, M. P. Remington, P. J. Young, C. L. Lorson, S. Ikebe, P. S. Fishman, and R. H. Brown. 2004. A survival motor neuron: tetanus toxin fragment C fusion protein for the targeted delivery of SMN protein to neurons. *Brain Res.* 995:84–96.
11. Falnes, P. O., and K. Sandvig. 2000. Penetration of protein toxins into cells. *Curr. Opin. Cell Biol.* 12:407–413.
12. Bennett, M. J., and D. Eisenberg. 1994. Refined structure of monomeric diphtheria toxin at 2.3 Å resolution. *Protein Sci.* 3:1464–1475.
13. Steere, B. 2001. Characterization of high-order oligomerization and energetics in diphtheria toxin. PhD thesis. University of California, Los Angeles.
14. Bennett, M. J., S. Choe, and D. Eisenberg. 1994. Refined structure of dimeric diphtheria toxin at 2.0 Å resolution. *Protein Sci.* 3:1444–1463.
15. Louie, G. V., W. Yang, M. E. Bowman, and S. Choe. 1997. Crystal structure of the complex of diphtheria toxin with an extracellular fragment of its receptor. *Mol. Cell.* 1:67–78.
16. Weiss, M. S., S. R. Blanke, R. J. Collier, and D. Eisenberg. 1995. Structure of the isolated catalytic domain of diphtheria toxin. *Biochemistry.* 34:773–781.
17. Oh, K. J., L. Senzel, R. J. Collier, and A. Finkelstein. 1999. Translocation of the catalytic domain of diphtheria toxin across planar phospholipid bilayers by its own T domain. *Proc. Natl. Acad. Sci. USA.* 96:8467–8470.
18. Silverman, J. A., J. A. Mindell, H. Zhan, A. Finkelstein, and R. J. Collier. 1994. Structure-function relationships in diphtheria toxin channels: I. Determining a minimal channel-forming domain. *J. Membr. Biol.* 137:17–28.
19. Huynh, P. D., C. Cui, H. Zhan, K. J. Oh, R. J. Collier, and A. Finkelstein. 1997. Probing the structure of the diphtheria toxin channel. Reactivity in planar lipid bilayer membranes of cysteine-substituted mutant channels with methanethiosulfonate derivatives. *J. Gen. Physiol.* 110:229–242.
20. Wang, Y., S. E. Malenbaum, K. Kachel, H. Zhan, R. J. Collier, and E. London. 1997. Identification of shallow and deep membrane-penetrating forms of diphtheria toxin T domain that are regulated by protein concentration and bilayer width. *J. Biol. Chem.* 272:25091–25098.
21. Kachel, K., J. Ren, R. J. Collier, and E. London. 1998. Identifying transmembrane states and defining the membrane insertion boundaries of hydrophobic helices in membrane-inserted diphtheria toxin T domain. *J. Biol. Chem.* 273:22950–22956.
22. Senzel, L., M. Gordon, R. O. Blaustein, K. J. Oh, R. J. Collier, and A. Finkelstein. 2000. Topography of diphtheria Toxin's T domain in the open channel state. *J. Gen. Physiol.* 115:421–434.
23. Steere, B., and D. Eisenberg. 2000. Characterization of high-order diphtheria toxin oligomers. *Biochemistry.* 39:15901–15909.
24. Bell, C. E., P. H. Poon, V. N. Schumaker, and D. Eisenberg. 1997. Oligomerization of a 45 kilodalton fragment of diphtheria toxin at pH 5.0 to a molecule of 20–24 subunits. *Biochemistry.* 36:15201–15207.
25. Sharpe, J. C., and E. London. 1999. Diphtheria toxin forms pores or different sizes depending on its concentration in membranes: probable relationship to oligomerization. *J. Membr. Biol.* 171:209–221.
26. Kagan, B. L., A. Finkelstein, and M. Colombini. 1981. Diphtheria toxin fragment forms large pores in phospholipid bilayer membranes. *Proc. Natl. Acad. Sci. USA.* 78:4950–4954.
27. Gordon, M., and A. Finkelstein. 2001. The number of subunits comprising the channel formed by the T domain of diphtheria toxin. *J. Gen. Physiol.* 118:471–480.
28. Falnes, P. O., S. Choe, I. H. Madshus, B. A. Wilson, and S. Olsnes. 1994. Inhibition of membrane translocation of diphtheria toxin A-fragment by internal disulfide bridges. *J. Biol. Chem.* 269:8402–8407.
29. Falnes, P. O., and S. Olsnes. 1995. Cell-mediated reduction and incomplete membrane translocation of diphtheria toxin mutants with internal disulfides in the A fragment. *J. Biol. Chem.* 270:20787–20793.
30. Wu, Z., K. S. Jakes, B. S. Samelson-Jones, B. Lai, G. Zhao, E. London, and A. Finkelstein. 2006. Protein translocation by bacterial toxin channels: a comparison of diphtheria toxin and colicin Ia. *Biophys. J.* 91:3249–3256.
31. Ren, J., K. Kachel, H. Kim, S. E. Malenbaum, R. J. Collier, and E. London. 1999. Interaction of diphtheria toxin T domain with molten globule-like proteins and its implications for translocation. *Science.* 284:955–957.
32. Montecucco, C., E. Papini, G. Schiavo, E. Padovan, and O. Rossetto. 1992. Ion channel and membrane translocation of diphtheria toxin. *FEMS Microbiol. Immunol.* 5:101–111.
33. Lanzrein, M., O. Sand, and S. Olsnes. 1996. GPI-anchored diphtheria toxin receptor allows membrane translocation of the toxin without detectable ion channel activity. *EMBO J.* 15:725–734.
34. Ladokhin, A. S., R. Legmann, R. J. Collier, and S. H. White. 2004. Reversible refolding of the diphtheria toxin T domain on lipid membranes. *Biochemistry.* 43:7451–7458.
35. Chenal, A., P. Savarin, P. Nizard, F. Guillain, D. Gillet, and V. Forge. 2002. Membrane protein insertion regulated by bringing electrostatic and hydrophobic interactions into play. A case study with the translocation domain of diphtheria toxin. *J. Biol. Chem.* 277:43425–43432.
36. Zhan, H., J. L. Elliott, W. H. Shen, P. D. Huynh, A. Finkelstein, and R. J. Collier. 1999. Effects of mutations in proline 345 on insertion of diphtheria toxin into model membranes. *J. Membr. Biol.* 167:173–181.
37. Blewitt, M. G., J. M. Chao, B. McKeever, R. Sarma, and E. London. 1984. Fluorescence characterization of the low pH-induced change in diphtheria toxin conformation: effect of salt. *Biochem. Biophys. Res. Commun.* 120:286–290.
38. Cabiaux, V., R. Brasseur, R. Wattiez, P. Falmagne, J. M. Ruysschaert, and E. Goormaghtigh. 1989. Secondary structure of diphtheria toxin and its fragments interacting with acidic liposomes studied by polarized infrared spectroscopy. *J. Biol. Chem.* 264:4928–4938.
39. Penfold, J., and R. Thomas. 1990. The application of the specular reflection of neutrons to the study of surfaces and interfaces. *J. Phys. Condens. Matter.* 2:1369–1412.
40. Russell, T. 1990. X-ray and neutron reflectivity for the investigation of polymers. *Mater. Sci. Rep.* 5:171–271.
41. Als-Nielsen, J., D. Jacquemain, K. Kjaer, F. Leveiller, M. Lahav, and L. Leiserowitz. 1994. Principles and applications of grazing incidence x-ray and neutron scattering from ordered molecular monolayers at the air-water interface. *Phys. Rep.* 246:251–313.
42. Neville, F., M. Cahuzac, O. Konovalov, Y. Ishitsuka, K. Y. L. Lee, I. Kuzmenko, G. M. Kale, and D. Gidalevitz. 2006. Lipid headgroup discrimination by antimicrobial peptide LL-37: insight into mechanism of action. *Biophys. J.* 90:1275–1287.
43. Song, L., M. R. Hobaugh, C. Shustak, S. Cheley, H. Bayley, and J. E. Gouaux. 1996. Structure of staphylococcal alpha-hemolysin, a heptameric transmembrane pore. *Science.* 274:1859–1866.
44. Milne, J. C., D. Furlong, P. C. Hanna, J. S. Wall, and R. J. Collier. 1994. Anthrax protective antigen forms oligomers during intoxication of mammalian cells. *J. Biol. Chem.* 269:20607–20612.
45. Mitamura, T., S. Higashiyama, N. Taniguchi, M. Klagsbrun, and E. Mekada. 1995. Diphtheria toxin binds to the epidermal growth factor (EGF)-like domain of human heparin-binding EGF-like growth factor/diphtheria toxin receptor and inhibits specifically its mitogenic activity. *J. Biol. Chem.* 270:1015–1019.